Bestätigung der Metadaten/Metadata Approval Sheet

Sehr geehrte Autoren,
Bitte prüfen Sie diese Angaben sorgfältig. Sie sind für alle nachfolgenden Publikationswege (Print, Online, Abstracting und Indexing, Suchmaschinen etc.) relevant. Änderungen sind später nicht mehr möglich. Bitte führen Sie eventuelle Korrekturen in den beschreibbaren Feldern in der rechten Spalte aus. Bitte bestätigen Sie die Korrektheit der Daten, indem Sie das Feld unten anklicken.

Vielen Dank für Ihre Mitarbeit, De Gruyter

Dear author,
Please check these data carefully. They are relevant for all following publication processes in Abstracting and Indexing Services, search engines. They cannot be changed after publication. Please fill in your corrections within the editable fields in the right column. Please confirm the correct data by clicking the field below.

Thanks for your kind cooperation, De Gruyter

Article-Title: Supramolecular association in (μ_2-pyrazine)-tetrakis(N,N-bis(2-hydroxyethyl)dithiocarbamato)dizinc(II) and its di-dioxane solvate

Subtitle:

Author 1:

Surname: Jotani

First Name: Mukesh M.

Corresponding: yes

E-Mail: mmjotani@rediffmail.com

Affiliation: Department of Physics, Bhavan's Sheth R. A. College of Science, Ahmedabad, Gujarat 380001, India

Author 2:

Surname: Poplaukhin

First Name: Pavel

Corresponding: no

E-Mail: no

Affiliation: Chemical Abstracts Service, 2540 Olentangy River Rd, Columbus, OH 43202, USA

Author 3:

Surname: Arman

First Name: Hadi D.

Corresponding: no

E-Mail: no

Affiliation: Department of Chemistry, The University of Texas at San Antonio, One UTSA Circle, San Antonio, TX 78249-0698, USA

Author 4:

Surname: Tiekink

First Name: Edward R.T.

Corresponding: yes

E-Mail: edwardt@sunway.edu.my

Affiliation: Centre for Crystalline Materials, Faculty of Science and Technology, Sunway University, 47500 Bandar Sunway, Selangor Darul Ehsan, Malaysia

Data checked and receipted   **Date:**

Wenn Sie die Korrektheit der Daten nicht durch einen Haken bestätigen oder keine Änderungen in diesem Formular angeben, gehen wir davon aus, dass die angegebenen Daten korrekt sind.

If you don't confirm the correctness by checking the box or implement your corrections in this form, we have to presume that all data are correct.

Mukesh M. Jotani*, Pavel Poplaukhin, Hadi D. Arman and Edward R.T. Tiekink*

Supramolecular association in (μ$_2$-pyrazine)-tetrakis(N,N-bis(2-hydroxyethyl)dithiocarbamato)dizinc(II) and its di-dioxane solvate

Q1: Please check and confirm that bold, italic and Roman fonts have been applied correctly throughout

Abstract: The crystal and molecular structures of {Zn[S$_2$CN(CH$_2$CH$_2$OH)$_2$]$_2$}$_2$(pyrazine), (**1**), and its di-dioxane solvate, (**2**), are described. In each of these, the centrosymmetric, binuclear molecule features a five-coordinated, highly distorted square-pyramidal geometry based on a NS$_4$ donor set. The three-dimensional architectures in **1** and **2** are sustained by extensive networks of distinctive hydroxyl-O−H···O(hydroxyl) hydrogen bonding. The topology of the lattices are very different ▢ at of **2** having a more regular appearance. The dioxane molecules reside in channels defined by the host molecules in **2** but, do not make many significant interactions with the host. The fact that **1** exhibits a significantly greater packing efficiency and a higher density suggests **1** is more stable than **2**. The retention of dioxane in crystals of **2** probably reflects its intimate involvement in nucleation and high boiling point, meaning it is retained during crystallisation. Hirshfeld surface analyses were conducted and confirm the importance of the hydroxyl-O−H···O(hydroxyl) hydrogen bonding but, also reveal the presence of other interactions, most notably C−H···π(chelate) interactions.

Keywords: crystal structure analysis; Hirshfeld surface; hydrogen bonding; X-ray diffraction; zinc dithiocarbamate.

Introduction

The structural chemistry of metal dithiocarbamates ($^{-}$S$_2$CNRR′), both transition metal [1] and main group element [2], is well studied and is rich and diverse, certainly compared with related metal xanthates ($^{-}$S$_2$COR) [3] and metal dithiophosphates [$^{-}$S$_2$P(OR)$_2$] [4]; R,R′ = alkyl, aryl. In terms of supramolecular chemistry, owing to the presence of peripheral alkyl/aryl groups of the $^{-}$S$_2$CNRR′ anions, which are not capable of forming significant intermolecular interactions such as hydrogen bonding, their self-assembly is usually limited to secondary interactions [5, 6], occurring between the metal centre and sulfur atoms derived from neighbouring molecules and, from a crystal engineering perspective, steric effects are paramount in this regard [7]. A sure way to enrich the supramolecular potential of the dithiocarbamate ligand is to functionalise the R/R′ with hydrogen bonding capacity, e.g. acceptors such as pyridyl rings [8, 9]. Another approach is to add hydroxyl substituents to the R/R′ groups, e.g. hydroxyethyl groups [10].

In this context, recent studies on the zinc-triad elements have revealed interesting structural motifs, e.g. supramolecular isomers of the then unprecedented coordination polymer {Cd[S$_2$CN(iPr)CH$_2$CH$_2$OH]$_2$·solvent}$_n$ [11], the unusual retention of the {Cd[S$_2$CN(iPr)CH$_2$CH$_2$OH]$_2$}$_2$·dimer in a complex with (E)-2-(pyridin-3-yl-methylidene)hydrazin-1-ylidene]methyl}pyridine which coordinates in the monodentate mode [12] and in the structural diversity of mercury derivatives [13]. By far the greatest attention has been directed towards the structural chemistry of Zn-containing dithiocarbamate compounds containing at least one hydroxyethyl group. The structures of Zn(S$_2$CNRR′)$_2$ are usually dimeric owing to Zn−S bridges, i.e. {Zn(S$_2$CNRR′)$_2$}$_2$ but "isolated" in the crystalline state [7]. With hydrogen bonding functionality as in {Zn[S$_2$CN(CH$_2$CH$_2$OH)$_2$]$_2$}$_2$, the dimeric motif is retained but these associate via strong hydrogen bonding interactions into three-dimensional architectures in both characterised polymorphs which differ in the topology of layers, i.e. flattened [14] and undulating [15]. Reducing the hydrogen bonding potential as in {Zn[S$_2$CN(Et)CH$_2$CH$_2$OH]$_2$}$_2$ leads to supramolecular chains based on hydrogen bonding. Co-crystals can also be formed by these molecules as in case of {Zn[S$_2$CN(Me)CH$_2$CH$_2$OH]$_2$]$_2$}$_2$L^S where the bridging ligand L^S is (3-pyridyl)CH$_2$N(H)C(=S)C(=S)N(H)CH$_2$(3-pyridyl) [16]. When the co-crystal coformer is S$_8$, supramolecular

*Corresponding authors: Mukesh M. Jotani, Department of Physics, Bhavan's Sheth R. A. College of Science, Ahmedabad, Gujarat 380001, India, E-mail: mmjotani@rediffmail.com; and
Edward R.T. Tiekink, Centre for Crystalline Materials, Faculty of Science and Technology, Sunway University, 47500 Bandar Sunway, Selangor Darul Ehsan, Malaysia, E-mail: edwardt@sunway.edu.my
Pavel Poplaukhin: Chemical Abstracts Service, 2540 Olentangy River Rd, Columbus, OH 43202, USA
Hadi D. Arman: Department of Chemistry, The University of Texas at San Antonio, One UTSA Circle, San Antonio, TX 78249-0698, USA

layers are formed interspersed by S_8 molecules but when dimethylformamide is used, the oxygen atom disrupts the aforementioned hydrogen bonding leading to a one-dimensional chain instead [17]. Doubly interwoven coordination polymers are found in 2 : 1 adducts formed between $Zn[S_2CN(Me)CH_2CH_2OH)_2]_2$ and the oxygen analogue of L^S, i.e. L^O, and in the related 2 : 1 structure with the dimine dihydroxyl tautomer of L^O, i.e. $(3\text{-pyridyl})CH_2N = C(OH)$ $C(OH) = NCH_2(3\text{-pyridyl})$ [18]. While the importance of hydroxyl-O—H···O(hydroxyl) hydrogen bonding cannot be denied, sometimes hydroxyl-O—H···S(dithiocarbamate) hydrogen bonding is found instead [2☐]. The interesting structural chemistry notwithstanding, it is noted that some of the $\{Zn[S_2CN(R)CH_2CH_2OH)_2]_2\}_2$ species show anticancer potential, in particular when R = iPr [19]. In continuation of studies in this area, herein the crystal and molecular structures of $\{Zn[S_2CN(CH_2CH_2OH)_2]_2\}_2$(pyrazine) (**1**), Figure 1, and its dioxane di-solvate, $[\{Zn[S_2CN(CH_2CH_2OH)_2]_2\}_2$(pyrazine).2dioxane] (**2**), are described. The experimental study is complemented by a detailed analysis of the molecular packing by means of Hirshfeld surface analysis.

Experimental

Synthesis and characterisation

Compound **1** was prepared by dissolving bis[N,N-bis(2-hydroxyethyl)dithiocarbamato]zinc(II) [15] (1.0 mmol, 426 mg) and pyrazine (0.5 mmol, 40 mg) into a mixture comprising MeOH/EtOH (1 : 1 v/v). Crystals formed upon standing; M. pt: 409–411 K. Key IR bands (cm^{-1}): ν(C—N) 1470 (s) and ν(C—S) 1078 (m), 1043 (s). Crystallisation of **1** from dioxane resulted in the isolation of **2**.
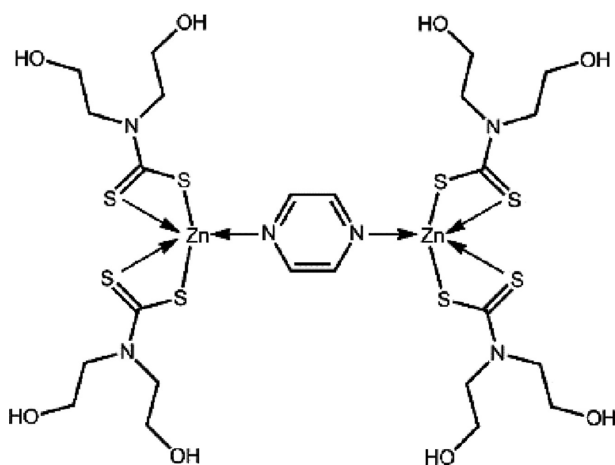

Fig. 1: Chemical diagram for the binuclear molecule in each of **1** and **2**.

Crystal structure determination

Intensity data for **1** and **2** were measured at 98 K on a Rigaku AFC12κ/SATURN724 diffractometer fitted with MoKα radiation. Data processing and absorption corrections were accomplished with CrystalClear [20] and ABSCOR [21], respectively. Details of cell data, X-ray data collection and structure refinement are given in Table 1. The structures were solved by Direct Methods [22]. Full-matrix least squares refinement on F^2 with anisotropic displacement parameters for all non-hydrogen atoms was performed [23]. The C-bound H atoms were placed on stereochemical grounds and refined with fixed geometries, each riding on a carrier atom, with anisotropic displacement parameter amounting to 1.2 times (1.5 for methyl-H) the value of the equivalent isotropic displacement parameter of the respective carrier atom. The O-bound H atoms were found in difference map and refined with O—H = 0.84 ± 0.01 Å, and with $U_{iso} = 1.5U_{eq}(O)$. A weighting scheme of the form $w = 1/[\sigma^2(F_o^2) + (aP)^2 + bP]$ where $P = (F_o^2 + 2F_c^2)/3$ was introduced in each case. For **1**, the maximum and minimum residual electron density peaks of 0.98 and 1.63 eÅ^{-3}, respectively, were located 1.04 and 0.65 Å from the Zn atom, respectively. In the refinement of **2**, four reflections, i.e. (10 12 0), (18 8 3), (13 4 2) and (9 4 3), were omitted owing to poor agreement. The authors note a level C CheckCIF alert arises for **2** to the effect that there is an 83% fit to a unit cell with $a/2$ for **2**. It is noted that the asymmetric unit of **2** comprises two independent half-molecules of $\{Zn[S_2CN(CH_2CH_2OH)_2]_2\}_2$(pyrazine), each located about a centre of inversion, and two dioxane molecules in general positions. Hence, it is possible to envisage a higher symmetry space group/phase transition. As discussed in the text, under the conditions of the X-ray diffraction experiment conducted on **2**, distinct molecular geometries are found for the zinc-containing molecules along with different patterns in the supramolecular associations. The programs WinGX [24], ORTEP-3 for Windows [24], PLATON [25], DIAMOND [26] and QMol [27] were also used in the study.

Hirshfeld surface analysis

The program *Crystal Explorer* 3.1 [28] was used to generate Hirshfeld surfaces mapped over d_{norm} for each of **1** and **2**. The contact distances d_i and d_e from the Hirshfeld surface to the nearest atom inside and outside, respectively, enable the analysis of the intermolecular interactions through the mapping of d_{norm}. The combination of d_e and d_i in the form of two-dimensional fingerprint plots [29] provides a useful summary of the most prominent intermolecular contacts operating in the respective crystals.

Results and discussion

Molecular structures

The molecular structure of **1** is shown in Figure 2 and selected geometric parameters are listed in Table 2. The molecular structure of the binuclear compound, i.e. $\{Zn[S_2CN(CH_2CH_2OH)_2]_2\}_2$(pyr), is situated about a centre

Tab. 1: Crystallographic data and refinement details for **1** and **2**.[a]

	1	2
Formula	$C_{24}H_{44}N_6O_8S_8Zn_2$	$C_{24}H_{44}N_6O_8S_8Zn_2.2(C_4H_8O_2)$
Formula weight	931.87	1108.08
Crystal colour, habit	Yellow, prism	Yellow, prism
Crystal size/mm	$0.15\times0.20\times0.26$	$0.05\times0.18\times0.22$
Crystal system	Triclinic	Monoclinic
Space group	$P\bar{1}$	$P2_1/c$
a/Å	8.8544(14)	28.610(6)
b/Å	9.7307(16)	11.784(2)
c/Å	11.3572(18)	14.116(3)
α/°	100.441(3)	90
β/°	95.455(2)	99.848(4)
γ/°	107.621(2)	90
V/Å³	905.4(3)	4688.9(16)
Z/Z'	1/0.5	$4/2\times0.5$ (complex) + 2 (solvent)
D_c/g cm⁻³	1.709	1.570
$F(000)$	482	2312
$\mu(MoK\alpha)$/mm⁻¹	1.840	1.441
Measured data	14550	26503
θ range/°	2.5–40.6	1.9–26.0
Unique data	10185	9106
R_{int}	0.021	0.075
Observed data ($I \geq 2.0\sigma(I)$)	9358	7578
R, obs. data; all data	0.051; 0.055	0.058; 0.074
a; b in wghting scheme	0.030; 1.296	0.053; 9.466
R_w, obs. data; all data	0.101; 0.105	0.140; 0.152
Largest difference peak and hole (Å⁻³)	0.98, −1.63	0.62, −0.64

[a]Supplementary Material: Crystallographic data (including structure factors) for the structures reported in this paper have been deposited with the Cambridge Crystallographic Data Centre as supplementary publication numbers CCDC-1507480 and 1507481. Copies of available material can be obtained free of charge, on application to CCDC, 12 Union Road, Cambridge CB2 1EZ, UK [fax: +44-(0)1223-336033 or e-mail: deposit@ccdc.cam.ac.uk].
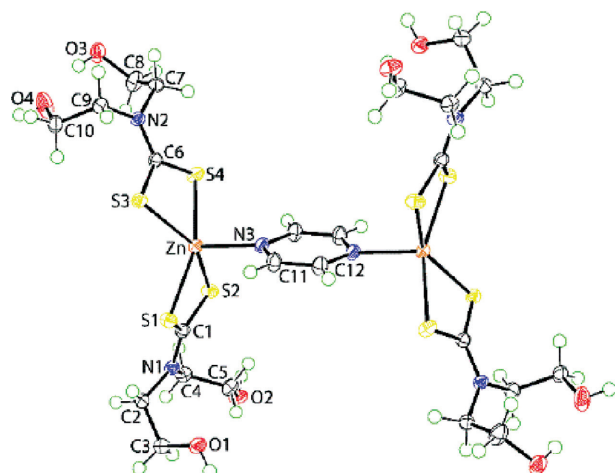

Fig. 2: Molecular structure of **1**. The molecule is disposed about a centre of inversion with unlabelled atoms related by symmetry operation *i*: −*x*, −*y*, −*z*. Displacement ellipsoids are drawn at the 70% probability level.

of inversion; pyr is pyrazine. The zinc(II) atom is chelated by two dithiocarbamate ligands and one nitrogen atom derived from the bidentate, bridging pyr ligand. The S1-dithiocarbamate ligand chelates the zinc atom forming different Zn−S bond lengths as seen in the value of Δ(Zn−S) of ca 0.05 Å, being the difference between the Zn−S$_{long}$ and Zn−S$_{short}$ bond lengths, Table 2. The S3-dithiocarbamate ligand coordinates with experimentally Zn−S bond lengths that lie within the values formed by the S1-ligand, Table 2. Reflecting the narrow range of Zn−S bond lengths, the associated C−S bond lengths are equal within experimental error. Hence, the zinc atom is five-coordinate within a NS$_4$ donor set. The value of τ is a well-accepted descriptor of five-coordinate coordination geometries [30]. A τ value of 0.0 corresponds to an ideal square pyramidal geometry while a value of 1.0 indicates an ideal trigonal pyramid. In **1**, τ computes to 0.19 indicating a distortion away from a square pyramid. In this description,

Tab. 2: Selected geometric parameters (Å, °) for **1** and **2**.

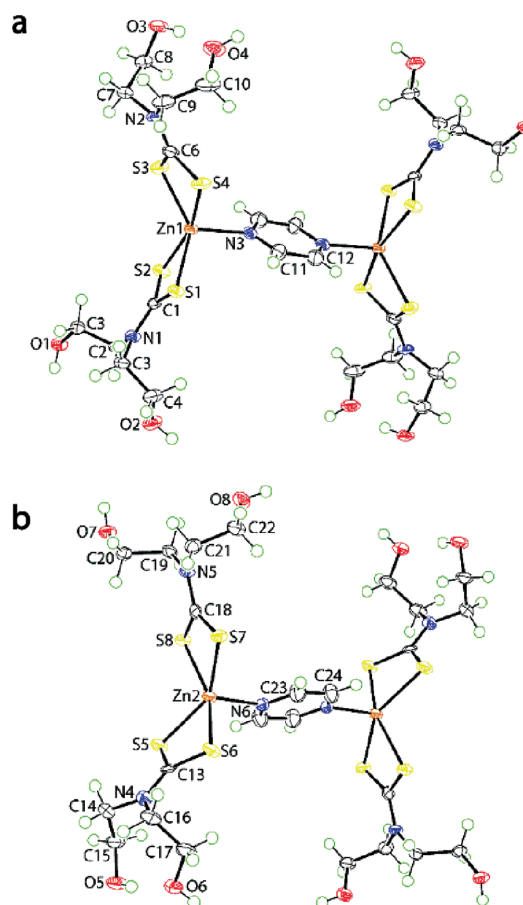|	1	2
Zn–S1	2.4121(6)	2.3733(10)
Zn–S2	2.4629(6)	2.4967(11)
Zn–S3	2.4496(5)	2.3772(10)
Zn–S4	2.4504(6)	2.4951(11)
Zn–N3	2.1419(13)	2.130(3)
Zn–S5	–	2.4019(10)
Zn–S6	–	2.4661(11)
Zn–S7	–	2.4055(10)
Zn–S8	–	2.4920(10)
Zn–N6	–	2.111(3)
C1–S1, S2	1.7254(15), 1.7245(15)	1.731(4), 1.720(4)
C6–S3, S4	1.7257(15), 1.7216(15)	1.724(4), 1.724(4)
C13–S5, S6	–	1.736(4), 1.723(4)
C18–S7, S8	–	1.725(4), 1.720(4)
S1, S2, C1/S3,S4,C6	45.10(11)	58.5(3)
S5, S6, C13/S7, S8, C18	–	56.6(3)
N1–C2–C3–O1	– 64.91(17)	166.9(3)
N1–C4–C5–O2	– 173.89(12)	67.2(4)
N2–C7–C8–O3	– 86.66(18)	73.3(4)
N2–C9–C10–O4	64.38(19)	– 61.9(4)
N4–C14–C15–O5	–	81.2(4)
N4–C16–C17–O6	–	– 68.1(4)
N5–C19–C20–O7	–	174.8(3)
N5–C21–C22–O8	–	65.4(4)

Fig. 3: Molecular structures in **2**; the solvent 1,4-dioxane molecules are omitted. Each molecule is disposed about a centre of inversion with unlabelled atoms related by symmetry operations: 1−x, 2−y, 1−z in (a) and 2−x, 1−y, 1−z in (b). Displacement ellipsoids are drawn at the 70% probability level.

the two approximately trans angles are 157.263(17)° for the S1–Zn–S4 angle and 146.018(16)° for S2–Zn–S3. The range of N3–Zn–S(n) angles is 98.61(4)° for n=1 to 115.22(4)° for n=3. Distortions from the ideal geometry relate in part to the acute chelate angles of 74.194(14) and 73.780(14)° for the four-membered chelate rings formed S1- and S3-dithiocarbamate ligands, respectively. Finally, the r.m.s. deviation of the four sulfur atoms from their least-squares plane is 0.1192 Å with the S1 and S4 atoms lying ca 0.12 Å to one side of the plane, and the S2 and S3 atoms lying ca 0.12 Å to the other side. The zinc atom lies 0.5984 (3) Å above the plane, in the direction of the N3 atom and to the same side as the S1 and S4 atoms.

The crystallographic asymmetric unit of **2** comprises two independent molecules of {Zn[S₂CN(CH₂CH₂OH)₂]₂}₂(pyr), each disposed about a centre of inversion, Figure 3, and two dioxane molecules of crystallization, each in a general position, to give the overall formulation {Zn[S₂CN(CH₂CH₂OH)₂]₂}₂(pyr).2dioxane. While to a first approximation, the coordination geometry in each of the independent Zn-containing molecules of **2** resembles that of **1**, some subtle differences are apparent. Referring to the data in Table 2, the obvious differences occurs in the magnitudes of the Zn–S bond lengths with the Zn–S$_{short}$ bonds in **2** being shorter than the equivalent bonds in **1**, especially for the Zn1-containing molecule, and in the

same way, the Zn–S$_{long}$ bonds are longer in **2** cf. **1**. These give rise to Δ(Zn–S) of 0.13 and 0.12 Å for the Zn1-molecule and 0.07 and 0.08 Å for the Zn2-molecule, all four values being greater than that observed for **1** of ca.0.05 Å. The values of τ [30] compute to 0.40 and 0.26, both indicating highly distorted coordination geometries but, closer to square pyramidal than trigonal pyramidal, and more distorted than observed for **1**. The Zn1 atom lies 0.5979(6) Å above the plane defined by the S₄ donor set (r.m.s. deviation=0.2318 Å) towards the N3 atom. The comparable values for the Zn2-containing molecule are 0.6358(6) and 0.1532 Å, respectively. Finally, it is noted that each dioxane molecule adopts a chair conformation.

The conformations of the dithiocarbamate ligands and the hydroxyethanol chains in **1** and **2** are quite variable as noted from the overlay diagrams in Figure 4, which have been drawn so that the central pyrazine rings are overlapped. The differences in the relative orientations
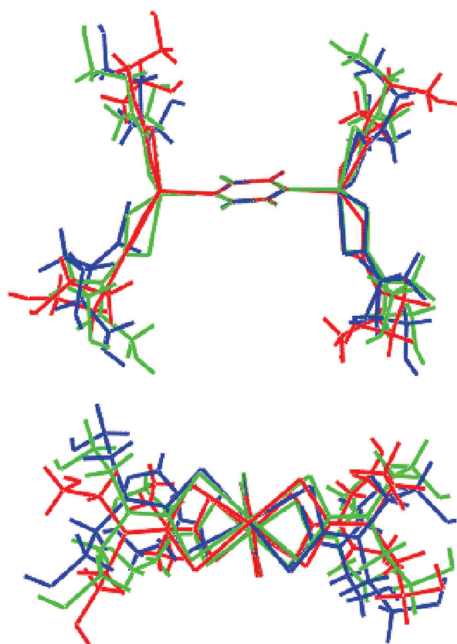
Fig. 4: Overlay diagrams of **1** (red image) and the two independent molecules in **2** (containing Zn1, green and Zn2, blue). The molecules have been superimposed so that the pyrazine molecules are coincident.

emphasise the different distorted coordination geometries as quantified, in part, by the dihedral angles between the chelate rings which vary by over 10°, Table 2. Torsion angle data for the N–C–C–O chains are included in Table 2. For

1, the asymmetric unit has one – anti-periplanar (-ap) conformation and three – syn-clinal (-sc) conformations implying the symmetry-related fragment has $1\times +$ap and $3\times +$sc conformations. In **2**, both asymmetric units have one $+$ap, $2\times +$sc and one $-$sc conformation. It is noted that the one $-$sc and two $+$sc conformations in the respective asymmetric units are very close to $+/-$ anti-clinal conformations and these correspond to the hydroxyethyl groups that form the donor intramolecular hydroxyl-O–H···O(hydroxyl) hydrogen bonds, see the next section.

Molecular packing

The molecular packing of **1** is dominated by hydroxyl-O–H···O(hydroxyl) hydrogen bonding with each hydroxyl group participating in one acceptor and one donor interaction as detailed in Table 3. Referring to Figure 5a, three key features are highlighted. Firstly, indicated by "1" in Figure 5a, is the formation of an intramolecular hydroxyl-O–H···O(hydroxyl) hydrogen bonding involving the O3–H and O4 atoms to close an eight-membered $\{\cdots HOC_2NC_2O\}$ loop. The hydroxyl groups of the other dithiocarbamate ligand associate about a centre of inversion via O1–H1o···O2 hydrogen bonds to generate a 16-membered $\{\cdots HOC_2NC_2O\}_2$ synthon, highlighted as "2" in Figure 5a. The third feature concerning the hydroxyl-O–H···O(hydroxyl) hydrogen bonding is the formation of

Tab. 3: Summary of intermolecular interactions (A–H···B; Å, °) operating in the crystal structures of **1** and **2**.

| A	H	B	A–H	H···B	A···B	A–H···B	Symmetry operation
1							
O1	H1o	O2	0.84(2)	1.85(3)	2.685(2)	173(3)	$-1-x, -y, 1-z$
O2	H2o	O3	0.838(19)	1.901(19)	2.735(2)	173(2)	$1-x, 1-y, 1-z$
O3	H3o	O4	0.84(3)	1.88(3)	2.701(2)	167(3)	x, y, z
O4	H4o	O1	0.84(3)	1.94(3)	2.716(2)	154(3)	$1+x, 1+y, z$
C2	H2a	S4	0.99	2.84	3.6000(18)	134	$-1+x, y, z$
C2	H2b	S2	0.99	2.84	3.6561(18)	140	$-x, 1-y, 1-z$
C7	H7a	Cg(Zn,S3,S4,C6)	0.99	2.82	3.5621(18)	132	$1-x, 1\text{-}y, -z$
2							
O1	H1o	O5	0.84(2)	1.91(3)	2.750(4)	177(4)	$-1+x, y, z$
O2	H2o	O7	0.84(3)	1.88(4)	2.696(4)	163(5)	$1-x, -\frac{1}{2}+y, \frac{1}{2}-z$
O3	H3o	O4	0.84(3)	1.82(3)	2.631(4)	165(4)	x, y, z
O4	H4o	O8	0.84(4)	1.89(4)	2.700(4)	163(5)	x, y, z
O5	H5o	O6	0.836(18)	1.84(2)	2.655(4)	165(4)	x, y, z
O6	H6o	O2	0.84(3)	1.86(3)	2.696(4)	171(4)	$1+x, y, z$
O7	H7o	O3	0.83(2)	1.92(3)	2.728(4)	162(4)	x, y, z
O8	H8o	O1	0.83(3)	1.87(3)	2.682(4)	163(4)	$1-x, -\frac{1}{2}+y, \frac{1}{2}-z$
C24	H24	S6	0.95	2.85	3.654(4)	143	$x, 1\frac{1}{2}-y, \frac{1}{2}+z$
C4	H4a	O9	0.99	2.53	3.338(5)	138	x, y, z
C7	H7b	Cg(Zn1,S1,S2,C1)	0.99	2.69	3.618(4)	156	$1-x, 2-y, -z$
C14	H14b	Cg(Zn2,S7,S8,C18)	0.99	2.62	3.560(4)	158	$2-x, 2-y, -z$
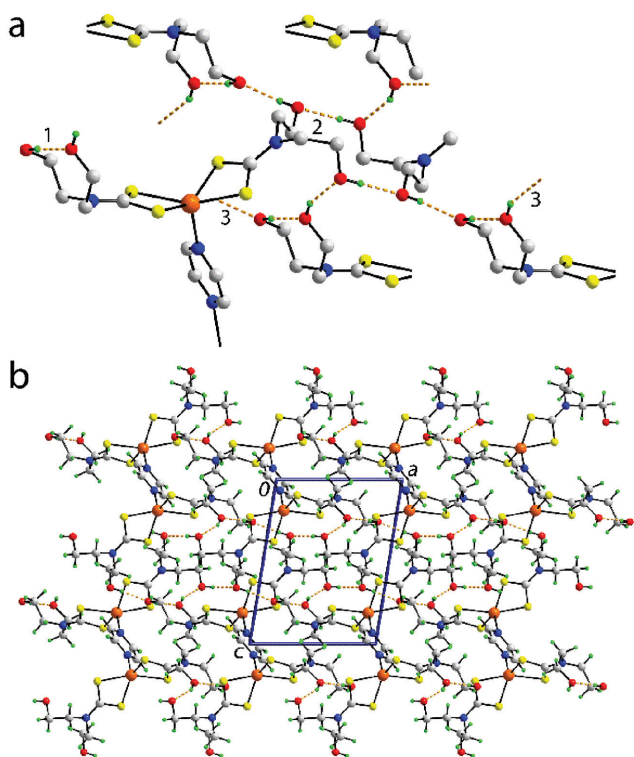
Fig. 5: Molecular packing in **1**: (a) detail of the hydroxyl-O–H⋯O(hydroxyl) hydrogen bonds, shown as orange dashed lines and (b) view of the unit cell contents shown in projection down the *b*-axis.
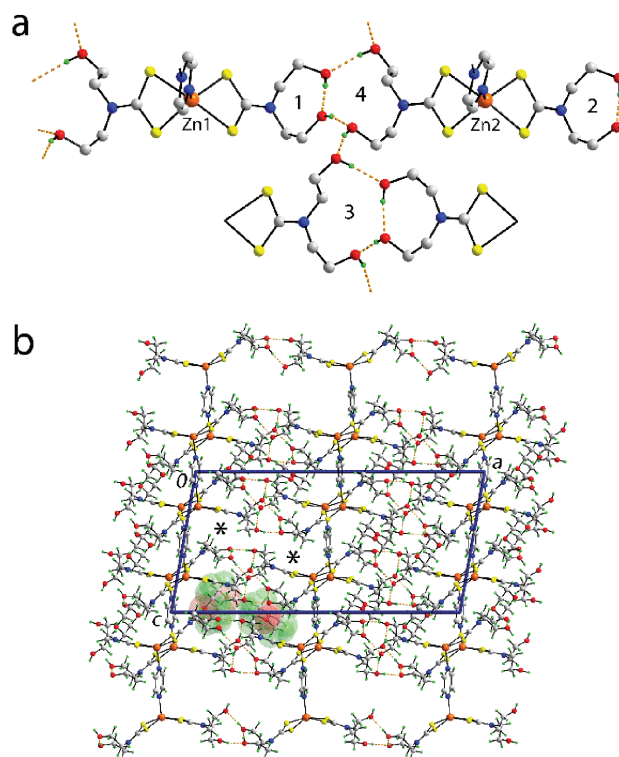

Fig. 6: Molecular packing in **2**: (a) detail of the hydroxyl-O–H⋯O(hydroxyl) hydrogen bonds, shown as orange dashed lines and (b) view of the unit cell contents shown in projection down the *b*-axis. In (b), the asterisks indicate vacant positions normally occupied by the dioxane molecules and dioxane molecules in one channel are highlighting in space-filling mode.

{⋯O1–H1o⋯O[ ]2o⋯O3–H3o⋯O4–H4o}$_n$ chains, see "3" in Figure [ ]. The net result of this association is the formation of a three-dimensional architecture, Figure 5b. Encompassed within this arrangement are reinforcing methylene-C–H⋯S interactions. Interestingly, the participating sulphur atoms in these interactions, i.e. S2 and S4, form the longer of the Zn–S bonds formed by each of the dithiocarbamate ligands, Table 2. Finally, based on the criteria in PLATON [25[ ]methylene-C–H⋯π(ZnS$_2$C), i.e. C–H⋯π(chelate ring) [3[ ], [ ]], interactions are apparent. The significance of the C–H⋯S, π interactions is probed further below, in the section "Hirshfeld surface analysis".

The molecular packing of **2** also features hydroxyl-O–H⋯O(hydroxyl) hydrogen bonding, again with each hydroxyl group participating in one acceptor and one donor interaction as just described for **1**, Table 3. An image detailing the salient features of the hydrogen bonding is shown in Figure 6a. Despite there being two independent molecules in the asymmetric unit, each exhibits common hydrogen bonding patterns. Thus, as indicated by "1" and "2" in Figure 6a, two of the dithiocarbamate ligands feature intramolecular hydroxyl-O–H⋯O(hydroxyl) hydrogen bonding to close a {⋯HOC$_2$NC$_2$O} loop, a pattern

noted for **1**. In **2**, these are formed by O3–H3o⋯O4 and O5–H5o⋯O6 atoms. Each of these O–H⋯O hydrogen bond bridges are incorporated into a larger synthon whereby the both hydroxyl groups of another dithiocarbamate ligand forms donor and acceptor hydrogen bonds with the hydroxyl groups of the bridge, see "3" and "4" in Figure 6a. This results in a non-symmetric 16-membered {⋯OC$_2$NC$_2$OH⋯OC$_2$NC$_2$OH} synthon whereby each of the original O–H⋯O bridges is now transannular. Links between these synthons are of the type hydroxyl-O–H⋯O(hydroxyl) with the O2 and O8 atoms being donors and the O7 and O1 atoms, respectively, being the acceptors, Table 3. This hydrogen bonding scheme leads [ ] three-dimensional architecture, Figure 6b, which is [ ] distinct from that adopted in **1**. Within this [ ]ework, pyr-C–H⋯S and methylene-C–H⋯π(ZnS$_2$C) [ ] found which are further analysed below in "Hirshfeld surface analysis".

The three-dimensional arrangement of the complex molecules in **2** is such to define channels parallel to the b-axis, in which reside the solvent dioxane molecules, Figure 6b. Curiously, the only identified interaction

between the host framework and solvent molecules within the standard distance criteria of PLATON [25], is a methylene-C–H⋯O9 contact, Table 3. The lack of strong interactions between a host lattice and dioxane is not unusual [32].

Simplified views of the molecular packing are presented in Figure 7. From this, it is evident that a considerable rearrangement of the molecular packing in **1** has been made to accommodate the dioxane guest molecules in **2**, resulting in a more regular, square-like framework.

The foregoing molecular packing poses the following question: what factors are responsible for disrupting the crystal structure of **1**? This is particularly salient given there are limited identifiable interactions between the host and guest molecules in **2** that might justify the adoption of a distinct packing arrangement. Further, in the crystal of **1** there is no significant solvent-accessible void apparent [25]. Indeed, the packing efficiency in **1** of 74.9% is significantly greater than that of **2**, which calculated to 1.6% [25]. This trend is also reflected in the calculated densities of 1.709 and 1.570 $g \cdot cm^{-3}$ for **1** and **2**, respectively. In the absence of other compelling reasons, it seems it is simply the chemical/physical nature of dioxane that is responsible for the adoption of the distinct molecular packing. Having a relatively high boiling point of ca

375 K [40], it is likely that the solvent simply "sticks" to the nucleating Zn-containing molecules and is not expelled during crystallisation.

Hirshfeld surface analysis

In order to gain a more thorough understanding of the molecular packing in **1** and **2**, and in particular to learn of the consequences of incorporating dioxane into the crystal of **2**, both structures were subjected to a Hirshfeld surface analysis.

In the view of the Hirshfeld surface mapped over d_{norm} in the range − 0.5 to + 1.1 au for **1**, Figure 8a, the bright-red spots are associated with the donors and acceptors of the respective O–H⋯O hydrogen bonds formed by the hydroxyl groups; these are labelled "1–3". Further mapping of Hirshfeld surfaces over d_{norm} in the range − 0.1 to + 1.1 au, Figure 8b, revealed the influence of the two methylene-C–H⋯S interactions as faint-red spots near the C2, S2 and S4 atoms; these are identified with labels "4" and "5". The red spot near atom S3, labelled with "6", indicates the presence of a short interatomic S⋯S contact, for data characterising this and other short interatomic contacts in the crystal of **1**, see Table 4. The faint-red
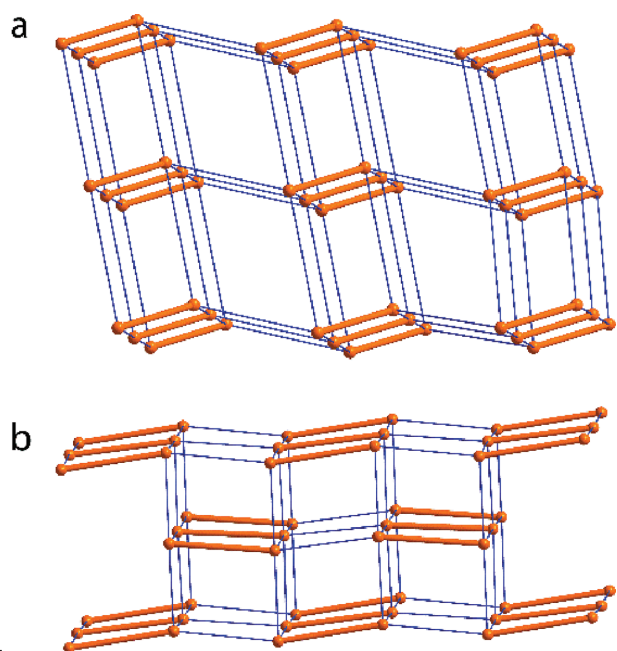
Fig. 7: Simplified views of the molecular packing of the Zn-containing molecules in (a) **1** (view ca down the b-axis) and (b) **2** (viewed ca down the a-axis). The dimers are represented by the golden rods. The apparent lack of symmetry in (b) reflects the presence of two independent binuclear molecules.
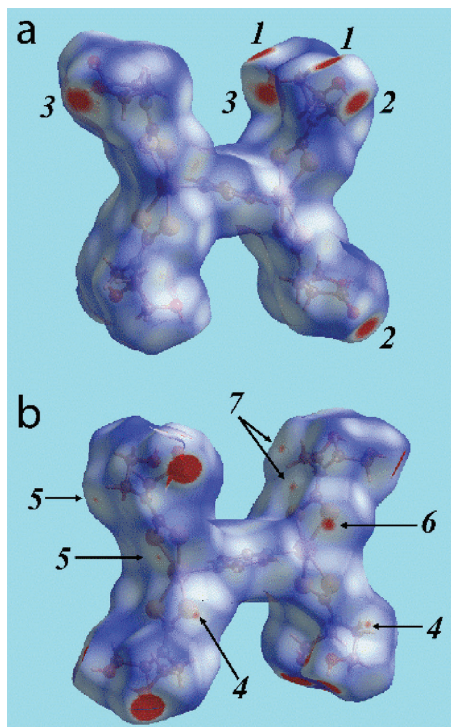

Fig. 8: Views of the Hirshfeld surfaces for **1** mapped over d_{norm} in the range (a) − 0.5 to + 1.1 au and (b) − 0.1 to + 1.1 au, highlighting the involvement of atoms in specific intermolecular interactions.

Tab. 4: Additional short contacts (Å) in **1** and **2**.

Contact	Distance (Å)	Symmetry Operation
1		
S3···S3	3.5078(8)	− x, 1 − y, − z
H4b···H6b	2.18	− 1+x, − 1+y, z
H1o···H4o	2.35(4)	− 1 − x, − y, 1 − z
H10···H5a	2.37	− 1 − x, − y, 1 − z
S1···H7b	2.96	− 1+x, y, z
S1···H8b	2.97	− 1+x, y, z
S1···H9a	2.91	− x, 1 − y, − z
C6···H7a	2.89	1 − x, 1 − y, − z
C6···C7	3.350(2)	1 − x, 1 − y, − z
Zn···H4a	3.34	− x, 1 − y, 1 − z
2		
H1o···H5o	2.34(5)	− 1+x, y, z
H2o···H6o	2.36(5)	− 1+x, y, z
H2o···H7o	2.28(5)	½ − x, − ½+y, ½ − z
H1o···H8o	2.23(5)	1 − x, ½+y, ½ − z
H3o···H7o	2.28(5)	x, y, z
H4o···H19b	2.28	x, y, z
H3b···H20b	2.27	1 − x, 2 − y, − z
H4b···H20b	2.38	1 − x, 2 − y, − z
H6o···H32b	2.36	x, 1+y, z
H15a···H29b	2.26	1+x, 1+y, 1 − z
O1···H21b	2.69	1 − x, 2 − y, − z
O6···H32b	2.69	1+x, 1½ − y, − ½+z
O7···H4b	2.64	1 − x, 2 − y, − z
O7···H28a	2.67	1 − x, 2 − y, − z
O10···H3a	2.67	x, − 1+y, z
O11···H27a	2.70	x, y, 1+z
O12···H17b	2.67	− 1+x, y, z
S1···H7b	2.94	1 − x, 2 − y, − z
S2···H10a	2.93	1 − x, ½+y, ½ − z
S4···H12	2.89	x, 1½ − y, − ½+z
S6···H31b	2.99	1+x, 1½ − y, − ½+z
S8···H17a	2.91	2 − x, ½+y, ½ − z
C1···H7b	2.84	1 − x, 2 − y, − z
C3···H8o	2.81(4)	1 − x, ½+y, ½ − z
C5···H6o	2.80(4)	− 1+x, y, z
C18···H14b	2.88	2 − x, 2 − y, − z
C18···H30a	2.67	1 − x, ½+y, ½ − z
C20···H2o	2.81(4)	1 − x, ½+y, ½ − z
C22···H4o	2.80(4)	x, y, z
C29···H15a	2.80	− 1+x, − 1+y, 1 − z
C29···H21a	2.85	1 − x, 1 − y, 1 − z
Zn1···H7b	3.17	1 − x, 2 − y, − z
Zn2···H14b	3.05	2 − x, 2 − y, − z
Zn1···C7	3.895(4)	1 − x, 2 − y, − z
Zn2···C14	3.794(4)	2 − x, 2 − y, − z

Fig. 9: A view of Hirshfeld surface mapped over d_{norm} for **1** showing O−H···O hydrogen bonds about a reference molecule. The hydrogen bonds are indicated with black dashed lines.

The presence of dioxane solvent molecules in a cavity of **2** can be clearly viewed from the Hirshfeld surface mapped over d_{norm}, shown in Figure 10.

The Hirshfeld surfaces generated for the individual Zn1- and Zn2-containing molecules in **2**, Figure 11a and b, resemble closely the overall shape observed for **1**, Figure 8. Again, the bright-red spots near the terminal hydroxyl groups indicate significant O−H···O hydrogen bonds, labelled "1–6". However, the presence of dioxane solvent molecules in **2** results in a three-dimensional architecture, Figure 12, very distinct from that in the structure of **1**, Figure 9, with the consequence that different intermolecular C−H···O and C−H···S interactions are observed

spots near methylene-C7 chelate ring-C6, labelled with "7", characterise the C−H···π(chelate) interaction. The immediate environment about the molecule within d_{norm} mapped Hirshfeld surface highlighting the hydrogen bonding connections is illustrated in Figure 9.
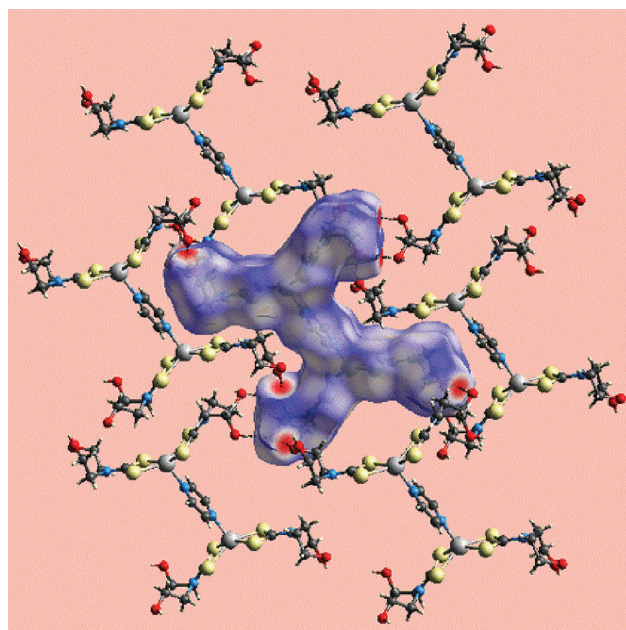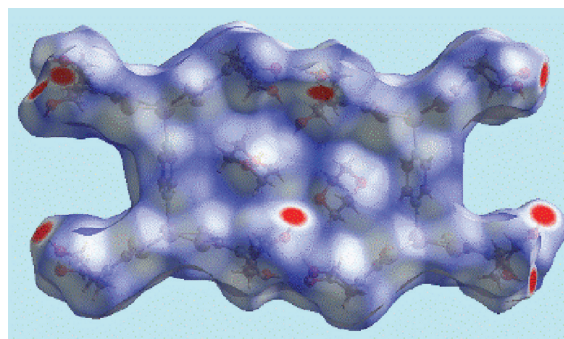

Fig. 10: A view of the Hirshfeld surface for **2**, mapped over d_{norm} in the range − 0.4 to 1.5 au, showing the two independent dioxane molecules within the cavity defined by the binuclear zinc-molecules.
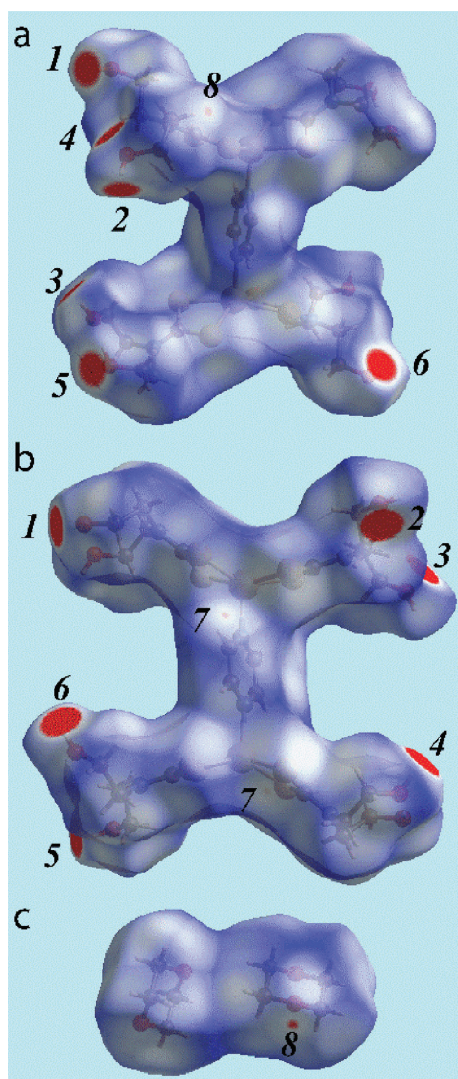
Fig. 11: Views of the Hirshfeld surfaces for **2**: (a) the Zn1-molecule (− 0.3 to + 1.3 au) (b) the Zn2-molecule (− 0.2 to + 1.3 au) and (c) the dioxane molecules (− 0.5 to + 1.4 au), mapped over d_{norm} highlighting the involvement of atoms in the intermolecular interactions.

Fig. 12: Two views of the Hirshfeld surfaces for **2**, mapped over d_{norm} highlighting the involvement of neighbouring atoms in the intermolecular interactions: (a) extended structure and (b) detail of the cavity containing the dioxane molecules.

in **2**. The presence of faint-red spots near methylene-C4, pyr-C24 and S6, labelled with "7", and near dioxane-O9, Figure 11c, labelled "8", result from the pyr-C24−H···S6 and methylene-C4−H4a···O9(dioxane) interactions, respectively.

The overall two dimensional fingerprint plots for **1**, individual Zn1- and Zn2-containing molecules of **2**, and for the full molecular system of **2**, i.e. comprising the both Zn1 and Zn2-molecules and the two dioxane molecules, are illustrated in Figure 13a. The respective plots have also been delineated into H···H, O···H/H···O, S···H/H···S, C···H/ H···C, S···S and Zn···H/H···Zn contacts [34], and are shown in Figures 13b−g, respectively; their relative contributions to the Hirshfeld surfaces are summarised in Table 5. The
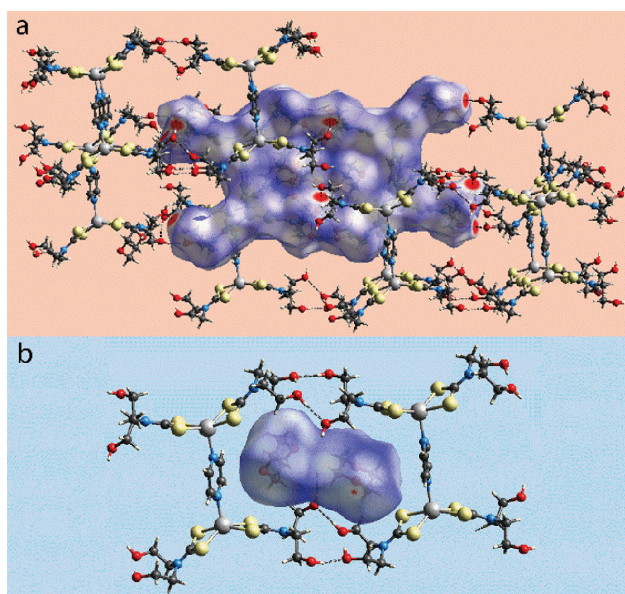
different shapes resulting from the distribution of points in the overall plots for **1** and **2**, Figure 13a, are clear indications of the formation of distinct three-dimensional arrangements in their crystals.

In the fingerprint plot delineated into H···H contacts for **1**, Figure 13b, a single peak at $d_e + d_i \sim 2.2$ Å arises from a short interatomic H···H contact between methylene-H4B and H7B atoms; the peaks for other two short contacts, Table 4, are diminished within the plot due to the overlap of points. For **2**, nearly the same percentage contribution from H···H contacts to the Hirshfeld surfaces of the Zn1- and Zn2-molecules and for the overall surface, Table 5, confirm that the solvent dioxane molecules occupy the free space between Zn-containing molecules. A small single peak at $d_e + d_i \sim 2.2$ Å in the plot for the Zn1-molecule and two nearly overlapping small peaks at $d_e + d_i \sim 2.3$ Å for the Zn2-molecule characterise the short interatomic H···H contacts between terminal hydroxyl groups, Table 4. The greater contribution from H···H contacts to the Hirshfeld surface of **2**, i.e. 51.0%, compared to 44.5% to **1**, most likely reflects the lack of specific intermolecular interactions involving the two dioxane molecules.

A pair of spikes with tips at $d_e + d_i \sim 1.8$ Å in the fingerprint plot delineated into O···H/H···O contacts for **1**, Figure 13c, represent the chain of O−H···O hydrogen bonds which give rise to the green points aligned as a pair. The similarity of the hydrogen bonding patterns involving the independent Zn1- and Zn2-molecules in **2** is reflected in the
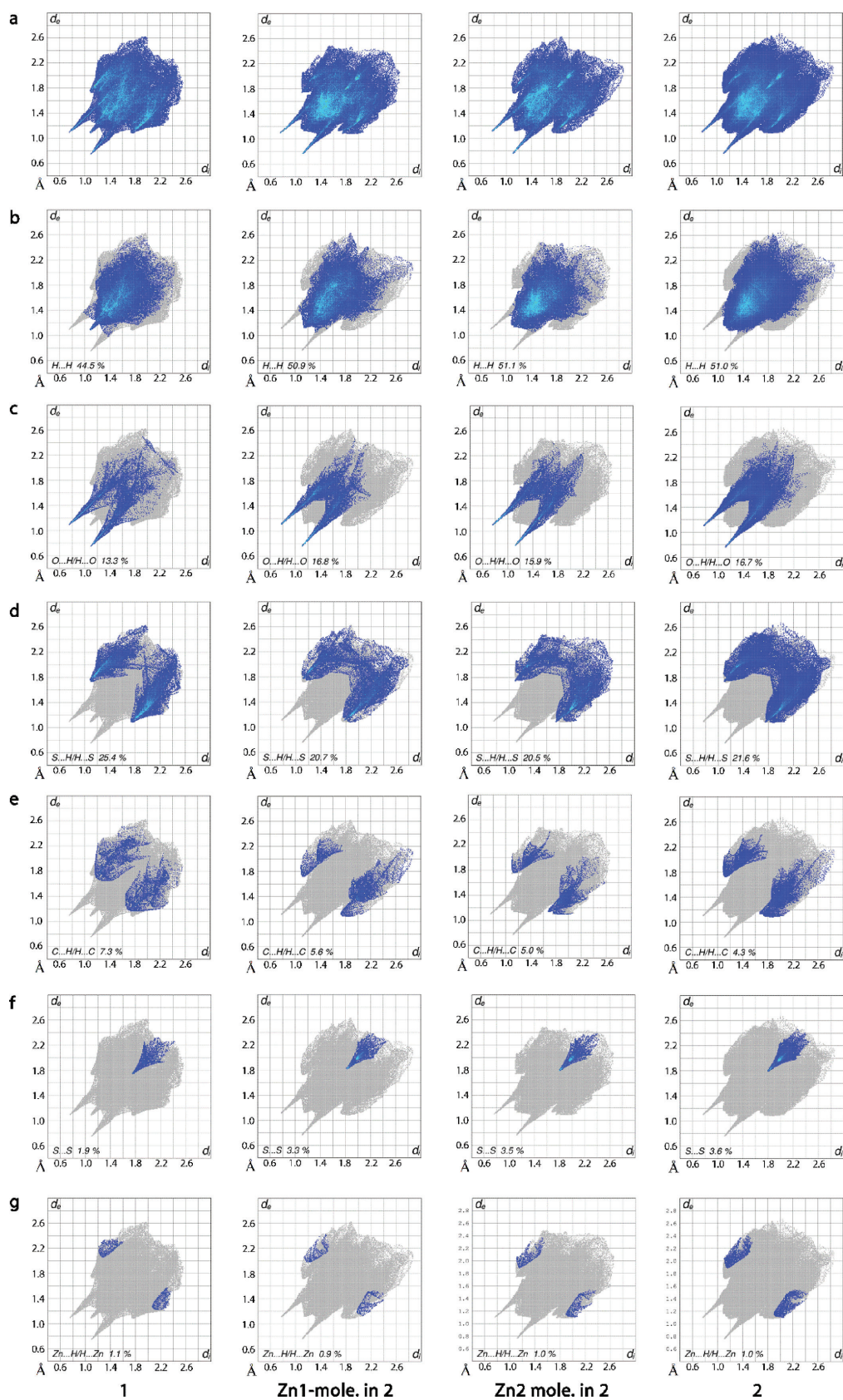
Fig. 13: Fingerprint plots calculated for **1,** the Zn1-molecule in **2**, the Zn2 molecule in **2** and **2**: (a) overall plots, and plots delineated into (b) H···H, (c) O···H/H···O, (d) S···H/H···S, (e) C···H/H···C, (f) S···S and (g) Zn···H/H···Zn contacts.

Tab. 5: Percentage contributions of various intermolecular contacts to the Hirshfeld surface areas of **1** and **2**.

Contact	% contribution			
	1	**2** (Zn1-mole)	**2** (Zn2-mole)	**2** (All)
H···H	44.5	50.9	51.1	51.0
O···H/H···O	13.3	16.8	15.9	16.7
S···H/H···S	25.4	20.7	20.5	21.6
C···H/H···C	7.3	5.6	5.0	4.3
S···S	1.9	3.3	3.5	3.6
Zn···H.H···Zn	1.1	0.9	1.0	1.0
N···H/H···N	3.6	1.4	1.0	0.9
C···O/O···C	1.5	0.1	1.1	0.3
C···N/N···C	0.2	0.0	0.0	0.0
N···O/O···N	0.1	0.0	0.7	0.2
N···S/S···N	0.0	0.2	0.2	0.2
S···O/O···S	1.1	0.0	0.0	0.1
O···O	0.0	0.1	0.0	0.1

similar appearance of their fingerprint plots delineated into O···H/H···O contacts and even to the pairs of spikes having tips at the same at $d_e + d_i$ distances, Figure 13c. However, the deviation of green points from the collinear alignments in the plots, cf. **1**, reflect the different hydrogen bonding network in **2**. The presence of short interatomic O···H/H···O contacts, Table 4, between the atoms of the dithiocarbamate ligand (host) and dioxane solvent (guest) in **2**, increases the percentage contribution from these contacts to their Hirshfeld surfaces; such interatomic contacts are absent in **1**. This fact is viewed as different densities of points in the respective plots.

The methylene-C–H···S interactions in **1** appear as a pair of sharp tips at $d_e + d_i \sim 2.8$ Å in the arrow-like plot corresponding to S···H/H···S contacts, Figure 13d. These interactions together with short interatomic S···H/H···S contacts, Table 4, result in a 24.5% contribution to the Hirshfeld surface of **1**. By contrast, the comparable fingerprint plots for both the Zn1- and Zn2-molecules of **2**, Figure 13d, have different shapes, cf. **1**, and a decrease in the percentage contribution to the Hirshfeld surface. A pair of small tips at $d_e + d_i \sim 2.8$ Å in the plot for the Zn2-molecule arise as a result of the pyr-C–H···S interaction. The bend in the plot for the Zn1-molecule plot at $d_e + d_i \sim 2.9$ Å is due to the involvement of the dithiocarbamate-S atom in the C–H···π(chelate) interaction and short interatomic S···H/H···S contacts, Table 4; the bend at $d_e + d_i \sim 3.0$ Å for the Zn2-molecule arises from similar interatomic contacts. The plot delineated into S···H/H···S contacts for the overall molecular system of **2** is just a superimposition of respective plots and shows a region with a high density of points.

In the fingerprint plot for **1** delineated into C···H/H···C contacts, Figure 13e, the points are distributed in such a way that the distance between them is greater than the sum of their van der Waals radii, whereas in the related plots for **2**, the peaks at $d_e + d_i \sim 2.8$ Å in the concave distribution of points are due to short interatomic C···H/H···C contacts involving atoms of the Zn-containing and solvent molecules, Table 4.

The similar shape of all of the fingerprint plots delineated into S···S contacts, Figure 13f, for both **1** and **2** and both show nearly identical distributions of points. This being stated, the interatomic S···S separations in **2** are equal to or greater than their van der Waals separations indicating the absence of such interactions in the molecular packing, whereas in the plot of **1**, the tip at $d_e + d_i \sim 3.5$ Å is the result of a short S3···S3 contact, Table 4.

The presence of short interatomic Zn···H/H···Zn contacts in both structures, Table 4, show they have a very small but measurable contribution to their respective Hirshfeld surfaces. Finally, the C–H···π(chelate) interactions observed in both molecular packings, see above, arise from the contributions of the S···H/H···S, C···H/H···C and Zn···H/H···Zn contacts, characterised as short interatomic distances, as listed in Table 4.

Conclusions

The centrosymmetric binuclear molecule, $\{Zn[S_2CN(CH_2CH_2OH)_2]_2\}_2$(pyrazine), (**1**), features a five-coordinated, distorted square-pyramidal geometry based on a NS_4 donor set. The three-dimensional architecture is sustained by an extensive network of hydrogen bonding. When recrystallised from dioxane, yielding **2**, crystals were found to contain two molecules of dioxane per binuclear zinc compound. Curiously, the three-dimensional architecture based on hydrogen bonding in **2** has a greater right-angle relationship between the three dimensions, cf. **1**, and the channels are occupied by dioxane molecules but, with limited specific intermolecular interactions between host and guest. The crystal data, e.g. density and packing efficiency, suggest that **2** is less stable than **1** bring into question why **2** forms at all. It is concluded that the dioxane molecules are involved in the nucleation process and with a high melting point, dioxane is retained during crystallisation of **2**.

References

[1]   P. J. Heard, *Prog. Inorg. Chem.* **2005**, *53*, 1.

[2]   G. Hogarth, *Prog. Inorg. Chem.* **2005**, *53*, 71.

[3]   E. R. T. Tiekink, I. Haiduc, *Prog. Inorg. Chem.* **2005**, *54*, 127.

[4]   I. Haiduc, D. B. Sowerby, *Polyhedron* **1996**, *15*, 2469.

[5]   N. W. Alcock, *Adv. Inorg. Chem. Radiochem*. **1972**, *15*, 1.

[6]   I. Haiduc, *Secondary Bonding* in J. L. Atwood, J. Steed, (Eds), *Encyclopedia of Supramolecular Chemistry*, Marcel Dekker Inc., New York, **2004**, pp. 1215.

[7]   E. R. T. Tiekink, *CrystEngComm*. **2003**, *5*, 101.

[8]   V. Singh, R. Chauhan, A. Kumar, L. Bahadur, N. Singh, *Dalton Trans*. **2010**, *39*, 9779.

[9]   V. Singh, A. Kumar, R. Prasad, G. Rajput, M. G. B. Drew, N. Singh, *CrystEngComm*. **2011**, *13*, 6817.

[10] R. A. Howie, G. M. de Lima, D. C. Menezes, J. L. Wardell, S. M. S. V. Wardell, D. J. Young, E. R. T. Tiekink, *CrystEngComm*. **2008**, *10*, 1626.

[11] Y. S. Tan, S. N. A. Halim, E. R. T. Tiekink, *Z. Kristallogr*. **2016**, *231*, 55.

[12] H. D. Arman, P. Poplaukhin, E. R. T. Tiekink, *Acta Crystallogr. E* **2016**, *72*, 1234.

[13] M. M. Jotani, Y. S. Tan, E. R. T. Tiekink, *Z. Kristallogr*. **2016**, *231*, 403.

[14] S. Thirumaran, V. Venkatachalam, A. Manohar, K. Ramalingam, G. Bocelli, A. Cantoni, *J. Coord. Chem*. **1998**, *44*, 281.

[15] R. E. Benson, C. A. Ellis, C. E. Lewis, E. R. T. Tiekink, *CrystEngComm* **2007**, *9*, 930.

[16] P. Poplaukhin, H. D. Arman, E. R. T. Tiekink, *Z. Kristallogr*. **2012**, *227*, 363.

[17] P. Poplaukhin, E. R. T. Tiekink, *CrystEngComm* **2010**, *12*, 1302.

[18] N. S. Jamaludin, S. N. A. Halim, C.-H. Khoo, B.-J. Chen, T.-H. See, J.-H. Sim, Y.-K. Cheah, H.-L. Seng, E. R. T. Tiekink, *Z. Kristallogr*. **2016**, *231*, 341.

[19] Y. S. Tan, K. K. Ooi, K. P. Ang, A. Md Akim, Y.-K. Cheah, S. N. A. Halim, H.-L. Seng, E. R. T. Tiekink, *J. Inorg. Biochem*. **2015**, *150*, 48.

[20] CrystalClear. User Manual. Rigaku/MSC Inc., Rigaku Corporation, The Woodlands, TX, 2005.

[21] Higashi, T.: ABSCOR. Rigaku Corporation, Tokyo, Japan, 1995.

[22] G. M. Sheldrick, *Acta Crystallogr. A* **2008**, *64*, 112.

[23] G. M. Sheldrick, *Acta Crystallogr. C* **2015**, *71*, 3.

[24] L. J. Farrugia, *J. Appl. Crystallogr*. **2012**, *45*, 849.

[25] A. L. Spek, *J. Appl. Crystallogr*. **2003**, *36*, 7.

[26] K. Brandenburg, DIAMOND. Crystal Impact GbR, Bonn, Germany, **2006**.

[27] J. Gans, D. Shalloway, *J. Molec. Graphics Model*. **2001**, *19*, 557.

[28] S. K. Wolff, D. J. Grimwood, J. J. McKinnon, M. J. Turner, D. Jayatilaka, M. A. Spackman, Crystal Explorer (Version 3.1), University of Western Australia, **2012**.

[29] J. J. McKinnon, M. A. Spackman, A. S. Mitchell, *Acta Crystallogr. B* **2004**, *60*, 627.

[30] A. W. Addison, T. N. Rao, J. Reedijk, J. van Rijn, G. C. Verschoor, *J. Chem. Soc. Dalton Trans*. **1984**, 1349.

[31] Y. S. Tan, S. N. A. Halim, K. C. Molloy, A. L. Sudlow, A. Otero-de-la-Roza, E. R. T. Tiekink, *CrystEngComm*. **2016**, *18*, 1105.

[32] V. Jayant, D. Das, *Cryst. Growth Des*. **2016**, *16*, 4183.

[33] *CRC Handbook of Chemistry and Physics*, ed. D. R. Lide, CRC Press, Boca Raton, 81st edn, 2000.

[34] J. J. McKinnon, D. Jayatilaka, M. A. Spackman, *Chem. Commun*. **2007**, 3814.

Q4: Please supply volume number refs. [30 and 34]

Q5: Ref. [33] is not cited in the text. Please supply text citation or delete the reference from the references list
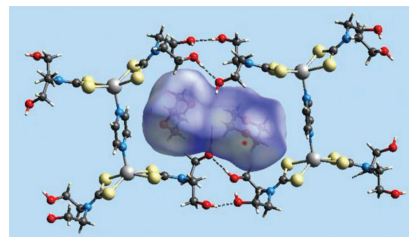
Graphical synopsis

Mukesh M. Jotani, Pavel Poplaukhin, Hadi D. Arman and Edward R.T. Tiekink

Supramolecular association in (μ₂-pyrazine)-tetrakis(N,N-bis(2-hydroxyethyl)dithiocarbamato) dizinc(II) and its di-dioxane solvate

Synopsis: Three-dimensional molecular packing based on hydroxyl-O–H⋯O(hydroxyl) is found in {Zn[S$_2$CN(CH$_2$CH$_2$OH)$_2$]$_2$}$_2$(pyrazine) and its dioxane solvate.